Syntheses, Structures, and Properties of Some Piano-Stool Iron Acetylides Bearing a Functional Anthracenyl Group

Frédéric de Montigny,[†,‡] Gilles Argouarch,[†] Thierry Roisnel,[†] Loic Toupet,[†] Claude Lapinte,[†,*] Sally Chan-Fung Lam,[§] Chi-Hang Tao,[§] and Vivian Wing-Wah Yam[§,*]

Sciences Chimiques de Rennes, UMR CNRS 6226, Université de Rennes 1, 35042 Rennes, France, Groupe Matière Condensée et Matériaux, UMR CNRS 6626, Université de Rennes 1, 35042 Rennes, France, and Centre for Carbon-Rich Molecular and Nano-Scale Metal-Based Materials Research and Department of Chemistry, The University of Hong Kong, Pokfulam Road, Hong Kong, People's Republic of China

Received December 21, 2007

The present study reports the isolation and the structural (X-ray), electrochemical (CV), and spectroscopic (IR, Mössbauer, ESR, UV–vis−NIR) characterization of the new complexes $[(\eta^2\text{-dppe})(\eta^5\text{-}C_5Me_5)Fe(-C{\equiv}C\text{-}9,10\text{-ant-}X)]^{n+}n[Y]$ (dppe = 1,2-bis(diphenylphosphino)ethane; ant = anthracene; n = 0, 1; **3a**^{n}Y, X = H; **3b**^{n}Y, X = Br; **3c**^{n}Y, X = CN; **3d**, X = C≡C−Si^{i}Pr$_3$; **3e**, X = C≡C−H; Y = PF_6, TCNE, TCNQ). It was shown that anthracene acts as a better transmitter than phenyl. The electron density on the Fe(III) nucleus depends on the distance between the metal center and the counteranion. The bulky $(\eta^2\text{-dppe})(\eta^5\text{-}C_5Me_5)Fe$ moiety is big enough to push the anthracene rings further apart and disrupts $\pi-\pi$ stacking except in the case of **3c**[TCNE] for which stacking is observed both between the TCNE anion and the (C_5Me_5) ligand and between anthracene fragments. The Fe(II) complexes display MLCT transitions in the 550–650 nm range while LMCT transitions can be observed in the 600–850 nm spectral range for the Fe(III) complexes. The Fe(II) and Fe(III) complexes exhibit weak luminescence property derived from the alkynyl anthracene units. Both Fe(II) and Fe(III) moieties can quench the ligand-centered emission by two different mechanisms.

Introduction

Considerable interest is now focused on the development of multifunctional molecular systems with synergetic properties.[1–4] In particular, assemblages incorporating redox and/or photoactive groups as a donor and/or acceptor have been the subjects of considerable recent research, as their attractive electronic and physical properties make them suitable candidates for switchable optical materials, [5–8] electrode surface modifiers,[9,10] and magnetic materials.[11–17]

Mononuclear organometallic acetylide complexes featuring one or several unpaired electrons exhibit usually a very rich chemistry and constitute a tremendous potential for molecular electronics, since redox-active organometallics stable under several oxidation states can be envisioned either as electron reservoirs or spin carriers.[18–20] This is particularly true for species containing the $(\eta^2\text{-dppe})(\eta^5\text{-}C_5Me_5)Fe(C{\equiv}C)-$ fragment,[21–28] owing to the potential these compounds offer for redox switching when incorporated in

* To whom correspondence should be addressed. E-mail: lapinte@univ-rennes1.fr; wwyam@hku.hk.

† University of Rennes 1.

‡ Present address: ENSCP-UMR7576, 11 rue Pierre et Marie Curie 75231, Paris Cedex 05, France.

§ The University of Hong Kong.

(1) Marder, S. R. *Inorganic Materials,* 2nd ed.; Wiley: Chichester, UK, 1996.

(2) Long, N. J. *Angew. Chem., Int. Ed.* **1995**, *34*, 21–38.

(3) Hudson, R. D. A. *J. Organomet. Chem.* **2001**, *637–639*, 47.

(4) Paul, F.; Lapinte, C. *Coord. Chem. Rev.* **1998**, *178–180*, 427–505.

(5) Samoc, M.; Gauthier, N.; Cifuentes, M. P.; Paul, F.; Lapinte, C.; Humphrey, M. G. *Angew. Chem.* **2007**, *45*, 7376–7379.

(6) Cifuentes, M. P.; Humphrey, M. G.; Morrall, J. P.; Samoc, M.; Paul, F.; Lapinte, C.; Roisnel, T. *Organometallics* **2005**, *24*, 4280–4288.

(7) Weyland, T.; Ledoux, I.; Brasselet, S.; Zyss, J.; Lapinte, C. *Organometallics* **2000**, *19*, 5235.

(8) Wong, K. M.-C.; Lam, S. C.-F.; Ko, C.-C.; Zhu, N.; Yam, V. W.-W.; Roué, S.; Lapinte, C.; Fathallah, S.; Costuas, K.; Kahlal, S.; Halet, J.-F. *Inorg. Chem.* **2003**, *42*, 7086–7097.

(9) Armstrong, N. R.; Carter, C.; Donley, C.; Simmonds, A.; Lee, P.; Brumbach, M.; Kippelen, B.; Domercq, B.; Yoo, S. *Thin Solid Films* **2003**, *445*, 342.

(10) Zou, C.; Wrighton, M. S. *J. Am. Chem. Soc.* **1990**, *112*, 7578.

(11) Sato, O.; Iyoda, T.; Fujishima, A.; Hashimoto, K. *Sciences* **1996**, *272*, 704.

(12) Nagai, K.; Iyoda, T.; Fujishima, A.; Hashimoto, K. *Solid State Commun.* **1997**, *102*, 809.

(13) Nakanishi, S.; Ojima, T.; Akutsu, H.; Yamada, J.-I. *J. Org. Chem.* **2002**, *67*, 916–921.

(14) Takeuchi, S.; Ogawa, Y.; Naito, A.; Sudo, K.; Yasuoka, N.; Akutsu, H.; Yamada, J.-I.; Nakatsuji, S. *Mol. Cryst. Liq. Cryst.* **2000**, *345*, 167.

(15) Nakatsuji, S.; Ogawa, Y.; Takeuchi, S.; Akutsu, H.; Yamada, J.-I.; Naito, A.; Sudo, K.; Yasuoka, N. *J. Chem. Soc., Perkin Trans.* **2000**, *2*, 1969.

(16) Nakatsuji, S.; Takahashi, S.; Ojima, T.; Ogawa, Y.; Akutsu, H.; Yamada, J.-I. *J. Mol. Cryst. Liq. Cryst.* **2001**, *356*, 23.

(17) Miller, J. S.; Epstein, A. J. *Angew. Chem., Int. Ed. Engl.* **1994**, *33*, 385–415.

(18) Venkatesan, K.; Blacque, O.; Fox, T.; Alfonso, M.; Schmalle, H.; Kheradmandan, S.; Berke, H. *Organometallics* **2005**, *24*, 920–932.

(19) Astruc, D. *Electron Transfer and Radical Processes in Transition-Metal Chemistry*; VCH: New York, 1995; p 630.

(20) Kahn, O. *Molecular Magnetism*; VCH Publishers, Inc.: New York, 1993; p 380.

(21) Le Narvor, N.; Toupet, L.; Lapinte, C. *J. Am. Chem. Soc.* **1995**, *117*, 7129–7138.

(22) Le Narvor, N.; Lapinte, C. *Organometallics* **1995**, *14*, 634–639.

(23) Weyland, T. Synthèse et Propriétés de Complexes Organo-fer Bi- et Tri-nucléaires sous differents degrés d'oxydation. Ph.D. Thesis, Rennes 1, Rennes, 1997.

(24) Weyland, T.; Costuas, K.; Mari, A.; Halet, J.-F.; Lapinte, C. *Organometallics* **1998**, *17*, 5569–5579.

(25) Weyland, T.; Costuas, K.; Toupet, L.; Halet, J.-F.; Lapinte, C. *Organometallics* **2000**, *19*, 4228–4239.

(26) Denis, R.; Toupet, L.; Paul, F.; Lapinte, C. *Organometallics* **2000**, *19*, 4240–4251.

(27) Costuas, K.; Paul, F.; Toupet, L.; Halet, J.-F.; Lapinte, C. *Organometallics* **2004**, *23*, 2053–2068.

10.1021/om701278e CCC: $40.75
Publication on Web 03/15/2008

Chart 1

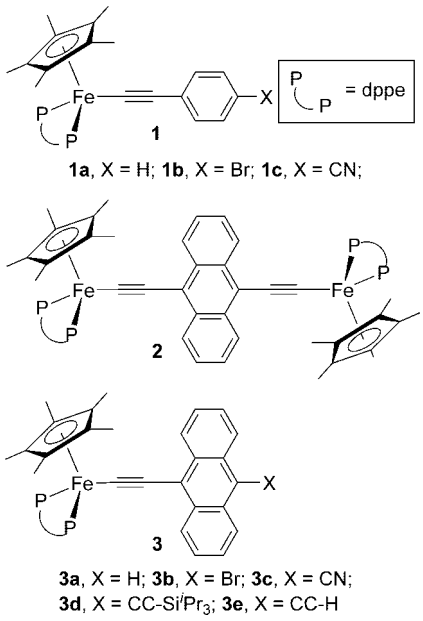

molecular devices.[4,29] In several instances, we have shown that this remarkable fragment allows efficient switching of various electronic properties of the complexes, such as ferromagnetic interactions,[24,25] fluorescence,[8] and nonlinear optical hyperpolarizability.[5,30,31] This effect results from the change in redox state of the iron center that is "transmitted" to the rest of the molecule through the alkynyl spacer. Mononuclear Fe(II)/Fe(III) compounds such as $[(\eta^2\text{-dppe})(\eta^5\text{-}C_5Me_5)Fe(C{\equiv}C{-}C_6H_4X)]^{n+}n[Y]$ have been extensively studied by some of us as model complexes to understand the influence of the substituents on the bonding properties within the metal−acetylide backbone (**1**, Chart 1).[28,32,33]

To introduce new functionalities in these complexes we have linked an anthracenyl moiety onto an iron alkynyl building block to generate the new series of complexes $[(\eta^2\text{-dppe})(\eta^5\text{-}C_5Me_5)Fe(C{\equiv}C\text{-}9,10\text{-}C_{14}H_8X)]^{n+}n[Y]$. Indeed, substituted anthracenes which possess a wide range of chemical and physical properties constitute very attractive building blocks for the construction of new multifunctional molecular devices with optical and magnetic properties. In particular, these compounds are known to dimerize upon irradiation in solution and/or in the solid state and the chromophoric system is therefore a promising system for investigating the change of magnetic properties in a spin system by their structural change upon irradiation.[34] On the other hand, it has been shown that very strong ferromagnetic coupling between organic radicals can be mediated through anthracene units.[35] The strong fluorescence of anthracenes constitutes also key properties for designing novel chemosensors and multifunctional materials.[36–38] The properties of anthracene derivatives to adsorb onto the side walls of single-walled carbon nanotubes (SWNTs) might open a route toward functional nanoparticles and supramolecular assemblies.[39] In a previous work we reported that the 9,10-bis(ethynyl)anthracene bridge mediates electron transfer and electron exchange between $[(\eta^2\text{-dppe})(\eta^5\text{-}C_5Me_5)Fe]^{n+}$ ($n = 0, 1$) building blocks (**2**, Chart 1). Taken as a whole, the experimental and theoretical data emphasized the specific role of the anthracene fragment, which allows good communication between the remote iron centers and favors the displacement of the spin density from the metal centers onto the α and β sp carbon atoms in the vicinity of the metal and the *ipso* carbon of the anthracene.[40]

In the course of our research to develop novel organometallics, we report here the synthesis of the neutral and radical cation complexes $[(\eta^2\text{-dppe})(\eta^5\text{-}C_5Me_5)Fe(-C{\equiv}C\text{-}9,10\text{-ant-}X)]^{n+}n[Y]$ (ant = anthracene; $n = 0, 1$; **3a**^{n}Y, X = H; **3b**^{n}Y, X = Br; **3c**^{n}Y, X = CN; **3d**, X = C≡C−Si^{i}Pr$_3$; **3e**, X = C≡C−H; Y = PF_6^-, $TCNE^-$, $TCNQ^-$). An extensive analysis of the properties of this new family of molecules including redox potentials, X-ray determination, and Mössbauer, vibrational, and electronic spectroscopies was achieved and the data were compared with those obtained for the mononuclear complexes $[(\eta^2\text{-dppe})(\eta^5\text{-}C_5Me_5)Fe(C{\equiv}C{-}C_6H_4X)]^{n+}n[Y]$. It was envisaged that the luminescence properties of the anthracenyl group would be perturbed, varied, or tuned by the electroswitchable iron(II)/iron(III) building block and the luminescent properties of **3a**^{n}[PF_6] and **3c**^{n}[PF_6] ($n = 0, 1$) were studied and compared.

Results

1. Synthesis of the Neutral Complexes 3a−e. The substituted Fe(II) σ-acetylide complexes **1** were essentially prepared by a Pd/Cu-catalyzed cross-coupling reaction between the iron acetylide $(\eta^2\text{-dppe})(\eta^5\text{-}C_5Me_5)FeC{\equiv}CH$ (**8**) and the corresponding substituted aryl bromide.[26] However, with the electron-rich $(\eta^2\text{-dppe})(\eta^5\text{-}C_5Me_5)Fe$ building block and a functional anthracene moiety the cornerstone of this chemistry rests in the recovery of the target products in a pure form. Indeed, chromatographic purification of the Fe(II) complexes proved detrimental in many cases and the presence of an anthracenyl group often limits the solubility of the material.

The optimization of the syntheses constitutes a prerequisite to limit the presence of side products at the lower level. For this reason we have compared the efficiency of the two possible routes to access to the complexes **3a−d**. The classical vinylidene route depicted in Scheme 1 (route A) can be carried out in the one-pot procedure by using trimethylsilylalkynylanthracene derivatives **4a−d** and the iron chloride **6**. Alternatively, the "metalla-Sonogashira" coupling reaction between the iron acetylide **8** and the haloanthracenes **5a−d** and **9** (route B) can be envisioned as a

(28) Paul, F.; Toupet, L.; Thépot, J.-Y.; Costuas, K.; Halet, J.-F.; Lapinte, C. *Organometallics* **2005**, *24*, 5464–5478.
(29) Paul, F.; Lapinte, C. Magnetic communication in binuclear organometallic complexes mediated by carbon-rich bridges. In *Unusual Structures and Physical Properties in Organometallic Chemistry*; Gielen, M., Willem, R., Wrackmeyer, B., Eds.; John Wiley & Sons: London, UK, 2002; pp 220–291.
(30) Weyland, T.; Ledoux, I.; Brasselet, S.; Zyss, J.; Lapinte, C. *Organometallics* **2000**, *19*, 5235–5237.
(31) Paul, F.; Costuas, K.; Ledoux, I.; Deveau, S.; Zyss, J.; Halet, J.-F.; Lapinte, C. *Organometallics* **2002**, *21*, 5229–5235.
(32) Costuas, K.; Paul, F.; Toupet, L.; Halet, J.-F.; Lapinte, C. *Organometallics* **2004**, *23*, 2053–2068.
(33) Paul, F.; da Costa, G.; Bondon, A.; Gauthier, N.; Sinbandhit, S.; Toupet, L.; Costuas, K.; Halet, J.-F.; Lapinte, C. *Organometallics* **2007**, *26*, 874–896.
(34) Bouas-Laurent, H.; Castellan, A.; Desvergne, J.-P.; Lapouyade, R. *Chem. Soc. Rev.* **2000**, *29*, 43.
(35) Kaneko, T.; Makino, T.; Miyaji, H.; Teraguchi, M.; Aoki, T.; Miyasaka, M.; Nishide, H. *J. Am. Chem. Soc.* **2003**, *125*, 3554–3557.
(36) Witulski, B.; Weber, M.; Bergsträsser, U.; Desvergne, J.-P.; Bassani, D. M.; Bouas-Laurent, H. *Org. Lett.* **2001**, *3*, 1467–1470.
(37) Carano, M.; Cicogna, F.; D'Ambra, I.; Gaddi, B.; Ingrosso, G.; Marcaccio, M.; Paolucci, D.; Pinzino, C.; Roffia, S. *Organometallics* **2002**, *21*, 5583.
(38) Cicogna, F.; Colonna, M.; Houben, J. L.; Ingrosso, G.; Marchetti, F. *J. Organomet. Chem.* **2000**, *593–594*, 251–266.
(39) Zhang, J.; Lee, J.-K.; Wu, Y.; Murray, R. W. *Nano Lett.* **2003**, *3*, 403–407.
(40) de Montigny, F.; Argouarch, G.; Costuas, K.; Halet, J.-F.; Roisnel, T.; Toupet, L.; Lapinte, C. *Organometallics* **2005**, *24*, 4558–4572.

Scheme 1[a]

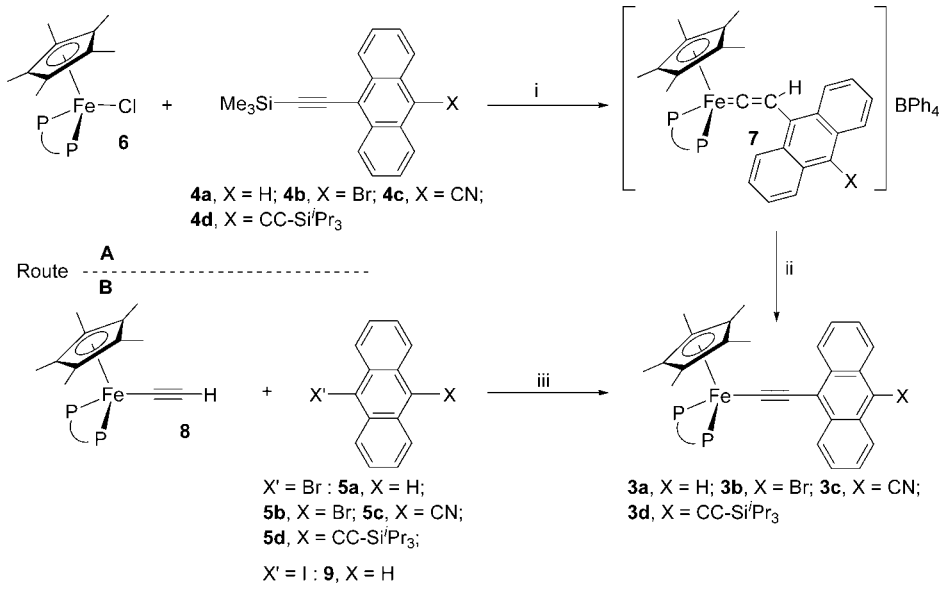

[a] Key reagents: (i) CH_3OH, K_2CO_3, $NaBPh_4$, 20 °C, 16 h; (ii) CH_3OH, $KOBu^t$, 20 °C, 4 h; (iii) $HN(^iPr)_2$, THF, $PdCl_2(PPh_3)_2$, CuI, 20–70 °C, 10 h.

Scheme 2[a]

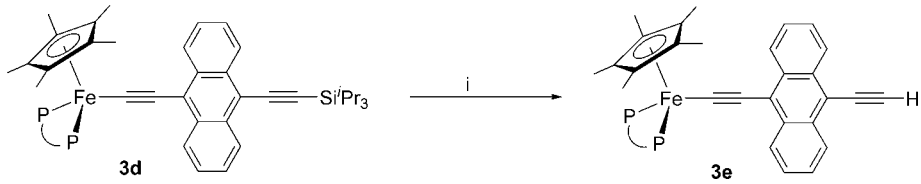

[a] Key reagents: (i) THF, TBAF, 50 °C, 16 h.

second pathway.[41] The organic anthracene-containing molecules were previously prepared and their syntheses separately reported.[42] Route A provides the complexes **3a** and **3b** in good yields, but the samples were always contaminated by a small amount of the corresponding terminal alkynes and their purification remained unsuccessful. This route is not suitable in the case of complex **3c**, the coordination of the nitrile being probably faster than the alkyne activation. However, complex **3d** was advantageously prepared by reaction of **6** with 9-triisopropylsilylethynyl-10-ethynylanthracene obtained from **4d** and isolated as a dark red powder in 57% yield.[42] The alternative route B did not allow the isolation of **3a**,**b** as pure samples, when **8** was reacted with **5a**,**b** in presence of the Pd/Cu catalysts. However, the more reactive iodide **9** provided **3a** in a pure form after washing with pentane (71%). The same route allowed the easy preparation of **3c** with a good yield (83%). In the case of complex **3b**, the oxidation with $[(\eta^5\text{-}C_5H_5)_2Fe][PF_6]$ of the contaminated material obtained by either route A or B gave **3b**$[PF_6]$ as a pure brown powder in 43–45% yield. The reversible reduction of **3b**$[PF_6]$ with $KOBu^t$ provides pure **3b** in 87% yield. Treatment of **3d** with TBAF in THF cleanly afforded complex **3e** as a pure red powder (82%, Scheme 2).

2. Characterization of the Neutral Complexes 3a−e. The neutral complexes were characterized by the usual spectroscopies and high-resolution LSI mass spectrometry, while X-ray data obtained for **3b** and **3c** confirmed the proposed structures (Figure 1). Satisfactory HRMS and/or elemental analyses were also obtained for most of these new compounds. All complexes were spectroscopically pure, as exemplified by the observation of a single ^{31}P NMR peak for the dppe ligand and a clean and sharp ^1H NMR signal for the methyl resonance of the C_5 ring. The low solubility of all these complexes precluded recording ^{13}C NMR spectra. The NMR data are in line with the usual features expected for complexes of the $(\eta^2\text{-dppe})(\eta^5\text{-}C_5Me_5)Fe$ series. The ^{31}P NMR shift spans a very narrow range between δ 100.8 and 101.8 and the ^1H NMR shift of $(\eta^5\text{-}C_5Me_5)$ remains between δ 1.55 and 1.68.

The complexes were also characterized by a typical infrared absorption at 1986–2022 cm^{-1}, which corresponds to the vibration mode of the C≡C bond coordinated to the iron center (Table 1). Another vibration mode was also observed at higher energy (2111–2118 cm^{-1}) for the complexes **3d** and **3e** and attributed to the noncoordinated C≡C−Si^iPr_3 and C≡C−H bonds. In a previous work on Fe(II) acetylides $(\eta^2\text{-dppe})(\eta^5\text{-}C_5Me_5)Fe(C{\equiv}C{-}C_6H_4{-}X)$ (**1**), we observed that the stretching frequency for the triple bond ($\nu_{C\equiv C}$) was dependent on the electronic nature of the appended substituent X and its evolution could be quantitatively rationalized by using a valence bond formalism, considering that electron-withdrawing substituents in Fe(II) acetylides favor the cumulenic character of the alkynyl bridge. Comparison of the previous results[26] with those obtained for the anthracene-containing series **3** indicates that the anthracene enhances the cumulenic character and increases the sensitivity to the electronic properties of X (Scheme 3). Indeed, the $\nu_{C\equiv C}$ frequencies decrease as the phenyl group is replaced

(41) Suzuki, H.; Kondo, A.; Inouye, M.; Ogawa, T. *Synthesis* **1986**, *1*, 121–122.

(42) de Montigny, F.; Argouarch, G.; Lapinte, C. *Synthesis* **2006**, 293–298.

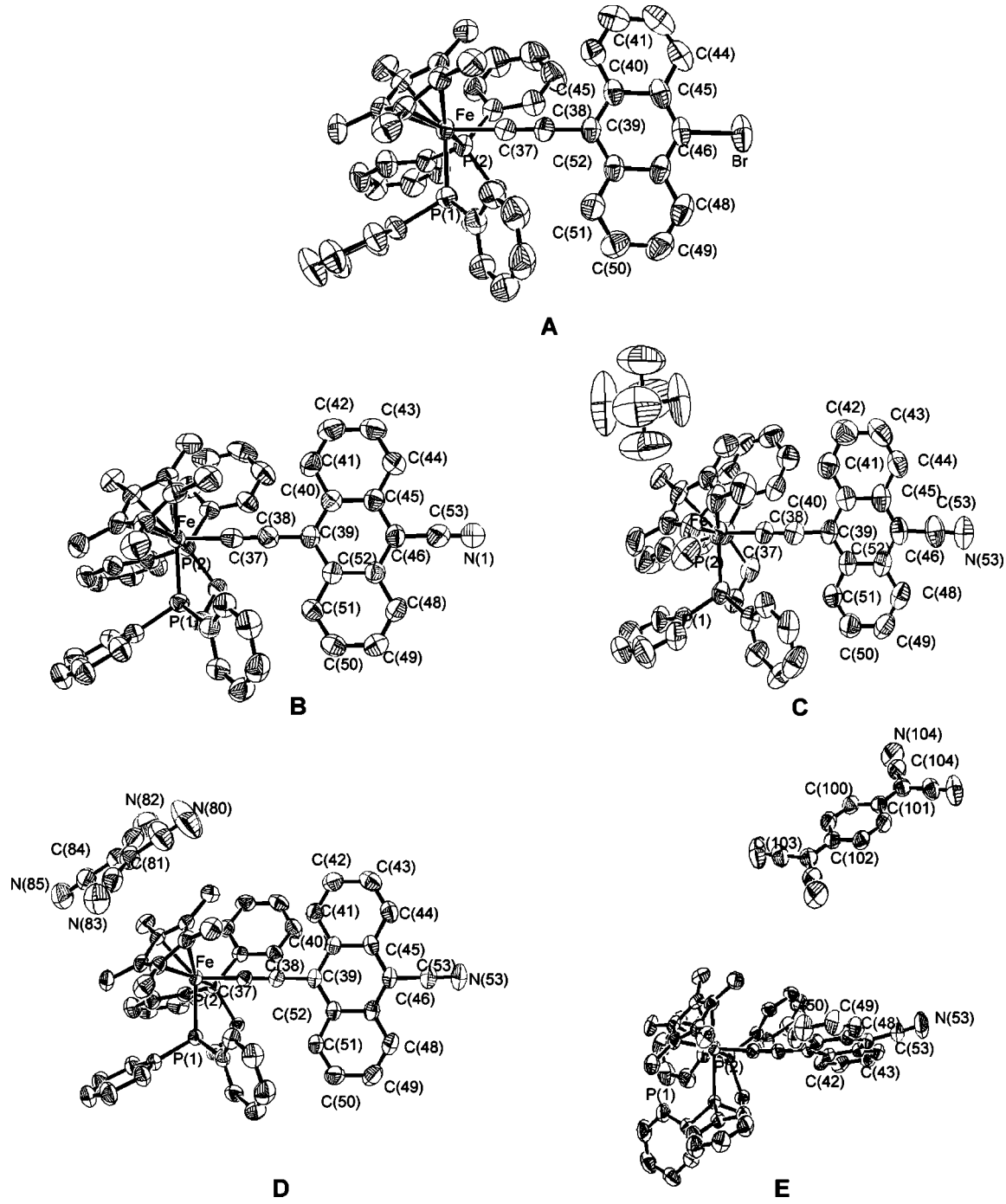

Figure 1. Drawings of **3b** (A), **3c** (B), **3c**[PF_6] (C), **3c**[TCNE] (D), and **3c**[TCNQ] (E) with selected atomic numbering. Thermal ellipsoids represented at the 50% probability level. Hydrogen atoms and solvent molecules are omitted for clarity.

by the anthracenyl fragment and the amplitude of the effect ($\Delta\nu_{C\equiv C}$) increases with the electron-withdrawing character of the X group from 31, 52, and 61 cm^{-1} for X = H, Br, and CN, respectively.

The cyclic voltammograms (CV) of all complexes display a reversible one-electron wave (Table 2) in the range 0.02 V/−0.13 V vs SCE, which corresponds to the Fe(II)/Fe(III) redox couple. A second irreversible process located before the solvent edge was observed around 1.0 V. This process involves more than one electron and could be assigned to an oxidation involving the anthracene fragment. Indeed, in the related series of complexes **1** a second irreversible process was observed at more positive potentials (1.35–1.40 V) and attributed to the Fe(III)/Fe(IV) couple. The reversible process corresponds to the well-known metal-centered Fe(II)/Fe(III) oxidation, and as expected it indicates that the Fe(III) analogues are stable at the platinum electrode. They constitute accessible synthetic targets. It is apparent that the presence of an electron-withdrawing substituent on the anthracene fragment makes the oxidation of the metal center more difficult, and for the same substituent this effect is larger than in the related series **1**. These results corroborate the IR data.

3. Synthesis and Characterization of the Oxidized Complexes 3a−c[Y] (Y = PF_6, TCNE, TCNQ). The hexafluorophosphate salts of the Fe(III) cations were generated by chemical oxidation of the neutral parents (**3a−c**), using 1 equiv of $[(C_5H_5)_2Fe][PF_6]$, and they were isolated as air-sensitive, but thermally stable powders. The color of the salts depends on the

Table 1. IR Frequencies (cm^{-1}) for Selected Fe(II) and Fe(III) Complexes in Nujol and CH_2Cl_2[a]

compd	Fe(II)	Fe(III)[b]	$\Delta\nu_{C\equiv C}$	ref
1a	(2053)	(2021)	−32	26
		(1988)	−65	
1b	2053 (2054)	(2017)	−37	26
1c	2047 (2048)	not obsd		26
	2028			
3a	2022	2018	−4	this work
3b	2001	1957	−44	this work
3c	1986 (1968)	1976 (1965)	−10	this work
		1977 (1966, 1992)[c]	−9	
		1951 (1967, 1992)[d]	−35	
3d	2118			this work
	1998			
3e	2111			this work
	2011			

[a] Values in CH_2Cl_2 are given in brackets. [b] With PF_6^- counteranion unless specified. [c] TCNE as counteranion. [d] TCNQ as counteranion.

Scheme 3. Electronic Structures for 3 and 3^+

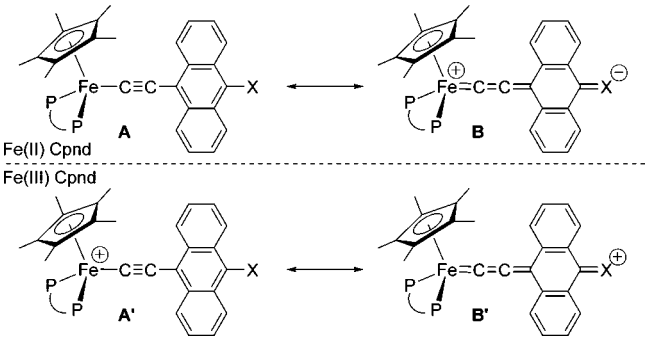

Table 2. Electrochemical Data for Selected Complexes

compd	ΔE_p	E_0[a]	i_c/i_a	ref
1a	0.08	−0.15	1	26
1b	0.08	−0.12	1	26
1c	0.08	−0.05	1	26
3a	0.08	−0.13	1	this work
3b	0.09	−0.08	1	this work
3c	0.08	0.02	1	this work
3d	0.08	−0.10	1	this work
3e	0.06	−0.11	1	this work

[a] All values in V vs SCE. Conditions: CH_2Cl_2, 0.1 M [^{n}Bu$_4$N][PF_6] supporting electrolyte, 20 °C, Pt electrode, sweep rate 0.100 V s^{-1}. The ferrocene/ferrocenium couple was used as internal reference for potentials measurements. E_0 values corrected for Fc/Fc^+ at 0.460 V vs SCE in CH_2Cl_2.

nature of the substituents X, and varies from dark blue to black and brown for **3a**[PF_6], **3b**[PF_6], and **3c**[PF_6], respectively. Furthermore, treatment of **3c** with 1 equiv of tetracyanoethylene (TCNE) or 7,7,8,8-tetracyanoquinodimethane (TCNQ) at –80 °C in THF provided the complexes **3c**[TCNE] and **3c**[TCNQ] which were isolated as brown (81%) and black (82%) powders, respectively. The redox potentials of TCNE and TCNQ being of 0.264 and 0.196 V vs SCE respectively, they were previously used as efficient reagents for the oxidation of related electron-rich metal complexes.[43] However, it is noteworthy that electron-deficient alkenes, such as TCNE, readily add to the C≡C triple bond adjacent to transition metals to give tetracyanocyclobutenyl, tetracyanobutadienyl, or allylic (vinylcarbene) complexes, according to conditions.[44–48] These alkenes can also be involved in Diels–Alder additions with anthracene and its analogues.[49–52] In the case of complex **3c**, the electron transfer is the unique observed reaction.

Table 3. ^{57}Fe Mössbauer Fitting Parameters at 80 K for Selected Complexes

compd	IS (mm s^{-1})	QS (mm s^{-1})	Γ (mm s^{-1})	ref
1a	0.28	2.02	na	26
1a[PF_6]	0.25	0.90	na	26
3a	0.264	1.945	0.134	this work
3a[PF_6]	0.110	0.825	0.213	this work
3b	0.251	1.883	0.129	this work
3b[PF_6]	0.116	0.927	0.192	this work
3c	0.239	1.863	0.131	this work
3c[PF_6]	0.242	0.913	0.199	this work
3c[TCNE]	0.259	0.849	0.146	this work
3c[TCNQ]	0.232	0.791	0.142	this work
3d	0.260	1.910	0.128	this work

Characterization of the Fe(III) derivatives was performed by the usual spectroscopic methods complemented for many of them by HRMS and/or elemental analysis. As expected, these dark compounds present a voltammogram identical with those obtained for their neutral parents, while their spectroscopic characteristics resemble those reported for **1a**−**c**[PF_6].[26,53] For the five complexes **3a**−**c**[PF_6], **3c**[TCNE], and **3c**[TCNQ], the IR absorption corresponding to the $\nu_{C\equiv C}$ stretch is shifted to lower wavenumbers relative to the respective neutral parents (Table 1, $\Delta\nu_{C\equiv C}$). This shift follows the same trend that was observed in the related series **1**. In addition, for **3c**[PF_6], the oxidation is evidenced by a 14 cm^{-1} shift of the C≡N stretching mode toward higher wavenumbers, indicating a decrease of the retrodonation of the anthracene group in the antibonding π^*(C≡N) orbital.

Some iron(II) and iron(III) complexes were also characterized by ^{57}Fe Mössbauer spectroscopy at 80 K. These results are reported in Table 3 and compared to measurements already found for **1a** and **1a**[PF_6].[26] Examination of the line width of the Mössbauer spectra reveals that broader lines were obtained for the compounds **3b**[PF_6] and **3c**[PF_6] (larger Γ values). The broadness of the lines suggests that the iron nuclei can exist in slightly different environments for these two compounds. In the case of the complex **3c**[PF_6] an X-ray crystal structure was obtained and two crystallographically different molecules were found in the unit cell (see below). One can assume that the line broadening probably has the same origin in the case of compound **3b**[PF_6].

The isomeric shift (IS) and quadrupolar splitting (QS) values found for the neutral complexes are very close to those previously obtained in the (η^2-dppe)(η^5-C_5Me_5)Fe—C≡C—R

(43) Roger, C.; Hamon, P.; Toupet, L.; Rabaâ, H.; Saillard, J.-Y.; Hamon, J.-R.; Lapinte, C. *Organometallics* **1991**, *10*, 1045–1054.
(44) Bruce, M. I.; Smith, M. E.; Skelton, B. W.; White, A. H. *J. Organomet. Chem.* **2001**, *484*, 637–639.
(45) Bruce, M. I.; Liddell, M. J.; Snow, M. R.; Tiekink, E. R. T. *Organometallics* **1987**, *7*, 343.
(46) Bruce, M. I.; Hambley, T. W.; Snow, M. R.; Swincer, A. G. *Organometallics* **1985**, *4*, 501.
(47) Bruce, M. I.; de Montigny, F.; Jevric, M.; Lapinte, C.; Skelton, B. W.; Smith, M. E.; White, A. H. *J. Organomet. Chem.* **2004**, *689*, 2860–2871.
(48) Bruce, M. I.; Low, P. J.; Hartl, F.; Humphrey, P. A.; de Montigny, F.; Jevric, M.; Lapinte, C.; Perkins, G. J.; Roberts, R. L.; Skelton, B. W.; White, A. H. *Organometallics* **2005**, *24*, 5241–5225.
(49) Atherton, J. C. C.; Jones, S. *Tetrahedron* **2003**, *59*, 9039.
(50) Bouas-Laurent, H.; Castellan, A.; Desvergne, J.-P.; Lapouyade, R. *Chem. Soc. Rev.* **2001**, *30*, 248.
(51) Kim, J. H.; Hubig, S. M.; Linderman, S. V.; Kochi, J. K. *J. Am. Chem. Soc.* **2001**, *123*, 87.
(52) Hashimoto, M.; Yamamura, K.; Yamane, J. *Tetrahedron* **2001**, *57*, 10253.
(53) Paul, F.; Mevellec, J.-Y.; Lapinte, C. *Dalton Trans.* **2002**, 1783–1790.

series.[54,55] However, one can note for the Fe(II) neutral complexes that the QS parameters are small suggesting a significant contribution of the mesomeric form B (Scheme 3) in the description of the electronic structure of the complexes **3**. Indeed, it has been shown in these series of complexes, the QS parameter is very sensitive to the nature of the Fe−C bond and usually decreases with the Fe−C bond distance.[55] The parameters determined for the cationic Fe(III) compounds are typical for 17-electron low-spin Fe(III) complexes. Probably, the contribution of the canonical form B′ (Scheme 3) is weak but significant in the description of the electronic structure of Fe(III) complexes and its weight, which depends on the nature of X, increasing in the order H < Br ≈ CN. In contrast with our observations for the binuclear complexes $\mathbf{2}^{+}$ and $\mathbf{2}^{2+}$ where the anthracenyl bridge favors the carbon character of the SOMO's,[40] in the mononuclear complexes **3** Mössbauer data do not suggest a significant spin distribution onto the ethynylanthracenyl ligand in contrast with reported results on ruthenium homologues.[56] Comparison of the previous results[26] with those obtained for the anthracene-containing series **3** indicates that the anthracene enhances the cumulenic character and increases the sensitivity to the electronic properties of X (Scheme 3).

Comparison of the IS and QS parameters obtained for **3c**[Y] (Y = PF_6, TCNE, TCNQ) shows the nature of the counteranion is sensed by the iron nucleus. The distant anions which surround the Mössbauer atom contribute to the total electric field (EFG) and consequently the QS values depend on their volume and symmetry.[57] The IS parameters reflect the electron density at the iron nucleus,[57] and should decrease as the distance between the iron nucleus and the anion increases. As expected, the smallest IS value is obtained for **3c**[TCNQ] for which the largest anion−cation distance was found (see below). In the case of the complexes **3c**[PF_6] and **3c**[TCNE] the distances between the iron center and the centroid of the anion are very similar, consequently, the IS values should be very close (see below). However, one can note that the IS parameter is larger in the case of **3c**[TCNE] indicating a stronger anion−cation interaction in this latter case. This was confirmed by the observation of a $\pi-\pi$ stacking interaction between the TCNE anion and the C_5Me_5 ligand as described in the next section.

4. Molecular Structures of 3b, 3c, 3c[PF$_6$], 3c[TCNE], and 3c[TCNQ]. Monocrystals of **3b**, **3c**, **3c**[PF_6], **3c**[TCNE], and **3c**[TCNQ] were grown, and the corresponding structures could be solved (Figure 1). The X-ray data are listed in Table 4 and the relevant bond distances and angles are given in Table 5. As invariably noted in the (η^2-dppe)(η^5-C_5Me_5)Fe series the iron centers exhibit octahedral geometry with bond lengths and angles in previously established ranges.[4,21,26,43,55] Comparison of the data obtained for Fe(II) and Fe(III) complexes shows the expansion of the coordination sphere upon oxidation as invariably observed for organoiron derivatives.[28] This is the major change associated with the reversible electron transfer. Only very small geometrical differences take place in the anthracenyl acetylide fragment when the oxidation state of the iron changes. The intermolecular Fe(II)−Fe(II) and Fe(III)−Fe(III) arrangements give 9.75, 11.01, 9.60, and 12.41 Å for the complexes **3c**, **3c**[PF_6], **3c**[TCNQ], and **3c**[TCNE], respectively, as shorter metal−metal distances.

Interestingly, comparison of the Fe−P distances in **3c**, **3c**[PF_6], **3c**[TCNE], and **3c**[TCNQ] reveals that the anion−cation interaction can play a significant role on the structure of the cation. Indeed, the Fe−P distances increase 3.8% from **3** to **3c**[PF_6] or **3c**[TCNE] and only 1.8% to **3c**[TCNQ]. It is also noteworthy that the distances between the cation and its anion strongly depend on the nature of the latter. In this trend, the distances between anion and cation decrease from 11.43 Å ($TCNQ_{cent}$−Fe) to 6.18/6.38 Å (PF_6−Fe) and to 5.41 Å ($TCNE_{cent}$−Fe, 293 K) and even to 5.32 Å for the same salt at 100 K. The increase of the cation–anion Coulombic interaction with the decrease of the cation–anion distance is corroborated by the increase of the IS parameter of the Mössbauer spectra, which reflects the increase of the electronic density at the iron nucleus in the order TCNQ < PF_6 < TCNE.

The apparent charge per TCNQ anion can be determined from the exocyclic double bond lengths.[58] They vary from 1.36 Å for TCNQ to 1.40 Å for $[TCNQ]^-$ and 1.43 Å for $[TCNQ]^{2-}$.[59] In **3c**[TCNQ], these distances (1.414(3) Å) are consistent with a full negative charge on the TCNQ anion. Similarly, in the case of TCNE, the central C═C bond elongates by 4% from 1.35 Å to 1.39 Å for a one-electron reduction[60] and to 1.49 Å for a two-electron reduction.[61] The observed C═C bond distance in **3c**[TCNE] of 1.404(5) Å at 293 K is also fully consistent with a full negative charge on the TCNE anion. Interestingly, X-ray diffraction data recorded at 100 K show that the central C═C bond length increases upon cooling (1.422(2) Å) suggesting that the degree of negative charge still increases when the temperature decreases. These results are consistent with both the redox potentials[43] and the Mössbauer QS values which are typical for iron(III) of these series.[54,55]

$\pi-\pi$ stacking is an important attribute of polyaromatic hydrocarbons like anthracenes which can affect different properties of the materials made from these compounds.[62] Thus special attention was paid to analyze these noncovalent $\pi-\pi$ interactions in the molecular structures of these complexes. The complexes **3b**, **3c**, **3c**[PF_6], and **3c**[TCNQ] do not exhibit any $\pi-\pi$ stacking in the solid state. Apparently, the presence of the bulky (η^2-dppe)(η^5-C_5Me_5)Fe moiety is sufficient to push the anthracene rings further apart and disrupt the $\pi-\pi$ stacking. However, analysis of the crystal structure of **3c**[TCNE] reveals an intermolecular $\pi-\pi$ stacking of the anthracene rings. The anthracene planes are parallel and the plane-to-plane distance is 3.437 Å at 100 K and slightly increases with temperature to 3.494 Å at 293 K. These values tend to be on the short side of usual range of 3.3–3.9 Å for such interactions.[63,64] The centroid−centroid vector length between stacked aromatic rings (4.080 Å) is longer than the plane-to-plane distance indicating a displacement between stacked rings. This degree of displace-

(54) Guillaume, V.; Thominot, P.; Coat, F.; Mari, A.; Lapinte, C. *J. Organomet. Chem.* **1998**, *565*, 75–80.
(55) Argouarch, G.; Thominot, P.; Paul, F.; Toupet, L.; Lapinte, C. *C. R. Chim.* **2003**, *6*, 209–222.
(56) Fox, M. A.; Roberts, R. L.; Khairul, W. M.; Hartl, F.; Low, P. J. *J. Organomet. Chem.* **2007**, *692*, 3277–3290.
(57) Gütlich, P.; Link, R.; Trautwein, A. *Mössbauer Spectroscopy and Transition Metal Chemistry*; Springer-Verlag: Berlin, Germany, 1978; Vol. 3, p 280.
(58) Miller, J. S.; Zhang, J. H.; Reiff, W. M.; Dixon, D. A.; Preston, L. D.; Reis, A. H.; Gebert, E.; Extine, M.; Troup, J.; Epstein, A.; Ward, M. D. *J. Am. Chem. Soc.* **1987**, *91*, 4344–4360.
(59) Hoekstra, A.; Spoelder, T.; Vos, A. *Acta Crystallogr.* **1972**, *B28*, 14–24.
(60) Miller, J. S.; Calabrese, J. C.; Rommelmann, H.; Chittipeddi, S. R.; Zhang, J. H.; Reiff, W. M.; Epstein, A. J. *J. Am. Chem. Soc.* **1987**, *109*, 769–781.
(61) Dixon, D. A.; Miller, J. R. *J. Am. Chem. Soc.* **1987**, *109*, 3656–3664.
(62) Goddard, R.; Haenel, M. W.; Herndon, W. C.; Kruger, C.; Zandler, M. **1995**, *117*, 30.
(63) Ionkin, A. S.; Marshall, W. J.; Wang, Y. *Organometallics* **2005**, *24*, 619.
(64) Ionkin, A. S.; Marshall, W. J.; Fish, B. M. *Organometallics* **2006**, *25*, 1461–1471.

Table 4. Crystallographic Data for 3b, 3c, 3c[PF_6], 3c[TCNE], and 3c[TCNQ]

	3b	**3c** · $2CH_2Cl_2$	**3c**[PF_6] · CH_2Cl_2	**3c**[TCNE] (293 K)	**3c**[TCNE] (100 K)	**3c**[TCNQ]
molecular formula	$C_{52}H_{47}BrFeP_2$	$C_{55}H_{51}Cl_4FeNP_2$	$C_{106}H_{90}Cl_2F_{12}Fe_2N_2P_6$	$C_{59}H_{47}Fe_1N_5P_2$	$C_{59}H_{47}Fe_1N_5P_2$	$C_{59}H_{49}Fe_1N_3P_2$
molecular wt	869.6	985.56	1988.22	943.81	943.81	917.8
cryst syst	monoclinic	orthorhombic	triclinic	monoclinic	monoclinic	monoclinic
space group	*C*2/*c*	*Pna*21	*P*1	*P*21/*n*	*P*21/*n*	*P*21/*c*
cryst color	black	blue	black	black	black	black
cell dimensions						
a, Å	28.473(5)	17.4990(2)	13.963(9)	12.228(5)	12.113(2)	14.979(5)
b, Å	17.184(5)	15.7403(2)	17.816(12)	24.575(5)	24.413(4)	16.927(5)
c, Å	21.298(5)	17.3715(2)	20.851(17)	17.099(5)	16.942(3)	19.189(5)
α, deg			78.59(3)			
β, deg	104.676(4)		73.71(3)	107.504(5)	108.092(5)	101.118(5)
γ, deg			82.38(2)			
V, Å^3	10081(4)	4784.86(1)	4863(6)	4900(3)	4762(2)	4774(2)
Z	8	4	2	4	4	4
d_{calcd}, g/cm^3 (293 K)	1.146	1.368	1.358	1.279	1.316	1.277
T (K)	293(2)	293(2)	293(2)	293(2)	100(2)	293(2)
abs coef (mm^{-1})	1.185	0.644	0.523	0.418	0.430	0.425
F(000)	3600	2048	2048	1968	1968	1920
crystdimensions (mm^3)	0.37 × 0.18 × 0.02	0.42 × 0.33 × 0.33	0.35 × 0.30 × 0.14	0.37 × 0.26 × 0.24	0.55 × 0.25 × 0.15	0.143 × 0.095 × 0.0508
diffractometer	Enraf Nonius FR590	Enraf Nonius FR590	Nonius Kappa CCD	Enraf Nonius FR590	APEX4 Bruker	Enraf Nonius FR590
radiation (Å)	Mo Kα 071069	Mo Kα 071069	Mo Kα 071073	Mo Kα 0.71073	Mo Kα 0.71073	Mo Kα 71069
data collection method	*ω*/2*θ*	*ω*/2*θ*	*ω*/2*θ*	*ω*/2*θ*	*ω*/2*θ*	*ω*/2*θ*
t_{max}/measure, s	60	60	60	60	60	60
range/indices (*h*,*k*,*l*)	−35, 35; –21, 21; −26, 26	0, 22; 0, 20; 0, 22	−17, 17; –22, 22; −26, 24	−15, 15; –31, 26; –22, 22	−11, 15; –31, 29; 29, -22	−19, 19; –21, 20; –24, 24
θ range	1.697 to 27.485	2.59 to 27.49	2.87 to 26.83	2.08 to 27.48	2.98 to 27.48	2.26 to 27.09
no. of reflns measd	10479	5666	25327	19893	56376	20381
no. of independent reflns	10330	5666	18395	11120	10903	10511
no. of obsd data, $I > 2\sigma(I)$	6410	5484	7750	6972	9484	8112
no. of variables	505	568	1189	604	604	583
final *R*	0.0845	0.0347	0.2119	0.0977	0.0385	0.0574
R_w	0.285	0.0915	0.338	0.1506	0.0932	0.118
R indices (all data)	0.1293	0.0329	0.094	0.0514	0.0385	0.04
GOF	1.083	1.044	1.008	1.012	1.057	1.036
largest diff peak	1.663	0.001	0.134	0.361	0.461	0.384
hole, eÅ^{-3}	−0.855	0.000	0.014	0.427	−0.312	0.429

Table 5. Selected Distances (Å) and Angles (deg) for 3b, 3c, 3c[PF_6], 3c[TCNE], and 3c[TCNQ]

				3c[TCNE]		
	3b	**3c**·$2CH_2Cl_2$	**3c**[PF_6]·CH_2Cl_2	293 K	100 K	**3c**[TCNQ]
$Fe(Cp^{*a})_{centroid}$	1.749	1.757	1.777/1.772	1.779	1.777	1.770
Fe−P1	2.181(2)	2.182(1)	2.265(2)/2.264(2)	2.2709(7)	2.2650(5)	2.2245(7)
Fe−P2	2.181(2)	2.182(1)	2.268(2)/2.266(2)	2.2675(7)	2.2690(5)	2.2291(7)
Fe−C37	1.887(5)	1.879(3)	1.878(7)/1.874(6)	1.886(2)	1.884(2)	1.872(2)
C37−C38	1.216(7)	1.234(4)	1.211(9)/1.227(9)	1.217(3)	1.220(2)	1.223(2)
C38−C39	1.442(7)	1.420(4)	1.428(9)/1.425(9)	1.435(3)	1.427(2)	1.423(2)
C39−C40	1.408(8)	1.425(4)	1.418(11)/1.429(11)	1.421(4)	1.419(2)	1.421(3)
C40−C41	1.409(9)	1.428(4)	1.378(12)/1.402(12)	1.424(4)	1.422(2)	1.419(3)
C41−C42	1.346(10)	1.363(5)	1.370(12)/1.394(12)	1.351(4)	1.362(2)	1.355(3)
C42−C43	1.366(11)	1.417(5)	1.439(14)/1.408(14)	1.412(4)	1.414(2)	1.407(3)
C43−C44	1.344(11)	1.371(5)	1.356(15)/1.340(14)	1.357(5)	1.361(2)	1.355(3)
C44−C45	1.435(10)	1.422(4)	1.407(12)/1.424(12)	1.425(4)	1.426(2)	1.417(3)
C45−C40	1.431(8)	1.436(4)	1.461(10)/1.422(10)	1.425(3)	1.428(2)	1.431(2)
C45−C46	1.393(10)	1.415(4)	1.373(12)/1.394(12)	1.406(4)	1.408(2)	1.409(3)
C46−C47	1.376(10)	1.410(4)	1.421(12)/1.410(11)	1.406(4)	1.405(2)	1.401(3)
C47−C52	1.466(8)	1.431(4)	1.433(9)/1.426(9)	1.434(3)	1.429(2)	1.432(3)
C52−C39	1.424(10)	1.425(4)	1.408(11)/1.402(10)	1.417(4)	1.422(2)	1.425(3)
C47−C48	1.414(10)	1.429(4)	1.410(12)/1.406(12)	1.419(4)	1.423(2)	1.422(3)
C48−C49	1.336(13)	1.361(4)	1.342(12)/1.370(12)	1.344(4)	1.358(2)	1.352(4)
C49−C50	1.408(13)	1.414(4)	1.418(11)/1.400(11)	1.410(4)	1.415(2)	1.404(4)
C50−C51	1.317(11)	1.370(4)	1.352(12)/1.348(11)	1.357(4)	1.363(2)	1.362(3)
C51−C52	1.424(10)	1.423(4)	1.422(10)/1.415(10)	1.412(4)	1.422(2)	1.418(3)
C46−C53/Br	1.912(5)	1.434(4)	1.436(10)/1.438(10)	1.445(3)	1.436(2)	1.435(3)
C53−N1		1.144(5)	1.146(9)/1.141(9)	1.131(3)	1.144(2)	1.133(3)
$(Cp^*)_{centroid}$Fe−P1	132.9	129.1	131.6/132.2	131.5	131.7	1.329
$(Cp^*)_{centroid}$Fe−P2	130.7	133.2	129.5/128.4	129.7	129.6	130.1
$(Cp^*)_{centroid}$Fe−C37	120.3	120.5	122.7/122.6	123.6	123.5	121.7
P1−Fe−P2	85.58(6)	85.61(3)	85.16(8)/84.73(8)	84.2(1))	83.98(2)	83.9(3)
P1−Fe−C37	86.90(17)	85.80(9)	87.8(3)/87.7(2)	89.3(1)	89.72(4)	87.3(1)
P2−Fe−C37	84.67(17)	87.81(9)	85.0(2)/86.7(2)	83.1(1)	82.74(4)	85.7(1)
Fe−C37−C38	179.4(6)	178.8(3)	177.2(6)/178.1(6)	177.9(2)	177.7(2)	177.6(2)
C37−C38−C39	172.3(6)	177.7(3)	178.2(7)/177.7(8)	177.4(3)	177.2(2)	176.7(2)
C40−C39−C52	119.3(6)	118.9(3)	121.0(7)/120.2(6)	120.4(2)	120.3(2)	119.7(2)
C45−C46−C47	123.8(5)	121.4(3)	124.0(7)/121.6(7)	122.5(2)	122.2(2)	122.3(2)
C45−C46−C53/Br	117.9(5)	119.5(3)	118.3(9)/119.7(8)	118.7(3)	118.5(2)	118.4(2)
C47−C46−C53/Br	118.2(5)	119.1(3°	117.6(9)/118.8(8)	118.8(3)	119.2(2)	119.2(2)
C46−C53−N1		179.3(4)	175.6(10)/177.8(10)	178.7(4)	178.7(2)	178.6(3)

[a] Cp* = (η^5-C_5Me_5).

ment between the rings can be defined by the β angle between the ring centroid vector and the ring normal to the plane of one aromatic ring. The value of β is 19.96° and the displacement between the rings compares well with data determined for other π-stacked aromatic rings.[65] Using the C_5Me_5 ligand on each molecule interacting in the dyad as a reference point for analyzing the conformation about the carbon-rich ligand and the centroid to define a torsion angle (θ), with $\theta = 180°$ and 0° corresponding to *anti* and *syn* arrangements, respectively, we see that compound **3c**[TCNE] shows an almost gauche arrangement of the terminal ends ($\theta = 80°$). This geometry is close to the conformation observed for the (η^2-dppe)(η^5-C_5Me_5)FeC≡CC≡CFe(η^5-C_5Me_5)(η^2-dppe) binuclear complex, but constitutes a notable difference from the analogue with a −C_8− all-carbon bridge[66] or the binuclear complexes **2c**$^{n+}$ ($n = 0, 1, 2$).[40] In addition, the crystal structure reveals anion−cation interaction. The C_5-ring–TCNE plane has a 6.4° dihedral angle, and the distance between the centroids of the C_5Me_5 ligand and TCNE anion is 3.595 Å.

5. ESR Spectroscopy. The X-band ESR spectra run at 77 K in a rigid glass ($CH_2Cl_2/C_2H_4Cl_2$, 1:1) for the complexes **3a**[PF_6] and **3c**[PF_6] display three well-resolved features corresponding to the components of the *g* tensor, as usually observed for d^5 low-spin iron(III) in pseudooctahedral geometry.[4,67] The *g* values extracted from the spectra are collected in Table 6, together with some *g* values of selected complexes of the (η^2-dppe)(η^5-C_5Me_5)Fe series. As observed in previous ESR investigations on similar compounds, the anisotropy tensor (Δg) of the ESR spectra increases with the electron-withdrawing capability of the substituents.[28] One can note that this sensitivity of the electronic properties to the substituents is larger in the anthracene series, which confirms that anthracene fragments act as better transmitters than phenyl rings. Note that the large isotropic tensor, $\langle g \rangle = {}^1/_3(g_1 + g_2 + g_3)$, and the large anisotropy of the signal ($\Delta g = g_3 - g_1$) confirm the large metallic character of the SOMO already deduced from the Mössbauer quadrupole splitting parameter. The spectra of **3c**[TCNE] and **3c**[TCNQ] displayed an extra signal corresponding to the paramagnetic anions observed at $g = 2.0027$ and 2.0019, respectively. The ESR spectra run with solid samples were poorly resolved.

Table 6. ESR Data[a] for Selected Fe(III) Complexes

compd	g_1	g_2	g_3	$\langle g \rangle$	Δg	ref
1a[PF_6]	1.975	2.033	2.464	2.157	0.489	28
1c[PF_6]	1.970	2.028	2.499	2.166	0.529	28
3a[PF_6]	1.978	2.037	2.412	2.195	0.434	this work
3c[PF_6]	1.973	2.027	2.496	2.234	0.523	this work
3c[TCNE]	1.976	2.032	2.483	2.164	0.507	this work
3c[TCNQ]	1.978	2.027	2.485	2.163	0.507	this work

[a] At 77 K in CH_2Cl_2−$C_2H_4Cl_2$ (1:1) glass.

(65) Cuffe, L.; Hudson, R. D. A.; Gallagher, J. F.; Jennings, S.; McAdam, C. J.; Connelly, R. B. T.; Manning, A. R.; Robinson, B. H.; Simpson, J. *Organometallics* **2005**, *24*, 2051–2060.

(66) Coat, F.; Paul, F.; Lapinte, C.; Toupet, L.; Costuas, K.; Halet, J.-F. *J. Organomet. Chem.* **2003**, *683*, 368–378.

(67) Rieger, P. H. *Coord. Chem. Rev.* **1994**, *135/136*, 203–286.

Table 7. UV–Vis Absorption and Emission Spectral Data of Complexes 1–3

complex	abs[a] λ/nm (10^3 ϵ/dm^3 mol^{-1} cm^{-1})	medium (T/K)	emission λ/nm (τ_o/μs)	Φ_{lum}	ref
1a	245 (34.0), 348 (13.6)		*b*	*b*	8
1a[PF_6]	241(sh, 34.0), 267 (37.0), 575 (2.2), 663 (2.9)		*b*	*b*	8
1c	267 (sh, 17.8), 281 (sh, 16.1), 387 (sh, 10.3), 445 (16.4)		*b*	*b*	26
1c[PF_6]	263 (sh, 40.5), 326 (sh, 12.5), 394 sh, 2.8), 458 (sh, 1.4), 501 (1.0), 652 (0.9)		*b*	*b*	26
2	268 (9.3), 334 (2.1), 391 (1.2), 410 (1.1), 622 (2.3)	CH_2Cl_2 (298)	441(<0.1)	1.82×10^{-3}	this work
		glass[c] (77)	394 (0.16)		
2[PF_6]	267 (11.1), 400 (2.1), 450 sh (1.4), 823 (4.8), 954 sh (1.8)	CH_2Cl_2 (298)	446(<0.1)	1.68×10^{-3}	this work
		glass[c] (77)	441 (0.17)		
2[PF_6]$_2$	265 (5.7), 408 (2.3), 468 (1.6), 818 (2.9)	CH_2Cl_2 (298)	445(<0.1)	3.59×10^{-4}	this work
		glass[c] (77)	393 (0.16)		
3a	260 (sh, 55.9), 372 (6.1), 553 (5.7)	CH_2Cl_2 (298)	404(<0.1)	3.95×10^{-3}	this work
		glass[c] (77)	401 (0.18)		
3a[PF_6]	266 (sh, 52.8), 399 (sh, 8.2), 534 (sh, 5.4), 604 (sh, 6.0), 884 (0.7), 1012 (1.0), 1887 (0.1)	CH_2Cl_2 (298)	466(<0.1)	1.11×10^{-2}	this work
		glass[c] (77)	420 (0.20)		
3c	268 (sh, 71.2), 320 (14.0), 396 (sh, 6.4), 602 (sh, 14.7) 651 (sh, 16.7)	CH_2Cl_2 (298)	426(<0.1)	7.75×10^{-3}	this work
		glass[c] (77)	449 (0.17)		
3c[PF_6]	272 (sh, 59.6), 399 (sh 9.2), 537 (sh, 9.1), 604 (sh 4.6), 441 (sh, 16.4), 896 (1.0), 1024 (1.4), 1974 (0.3)	CH_2Cl_2 (298)	433(<0.1)	3.74×10^{-3}	this work
		glass[c] (77)	425 (0.16)		

[a] Measured in CH_2Cl_2 at 293 K. [b] Not measured. [c] Measured in 2-methyltetrahydrofuran.

However, one can note the very weak intensity of the ESR signal obtained with solid samples of **3c**[TCNE] suggesting antiferromagnetic exchange interaction between the organometallic cation and the organic anion as observed in the crystal structure.

6. Uv–vis–NIR Absorption Spectroscopy. The UV–vis spectra of the neutral complexes were recorded in the range 250–900 nm. They resemble the spectra previously reported for the related *para*-substituent functionalized organoiron(II) compounds **1** (Table 7). Besides the high-energy transition at ca. 260−270 nm, which can apparently be attributed to $\pi-\pi^*$ ligand-centered transitions, less intense transitions were observed at ca. 370 nm for **3a** and 320 and 400 nm for **3c**. They constitute spectroscopic signatures of the anthracene fragment. Broad absorptions in the visible range are at the origin of the raspberry color of **3a** (553 nm) and dark blue color of **3c** (602 sh, 651 nm). Similar to the phenylethynyl series, these transitions can be assigned to MLCT transitions.[26] However, in comparison with **1a** and **1c** these transitions are red-shifted by ca. 200−215 nm, i.e., 7100−10500 cm^{-1}, for both compounds showing that 9,10-anthracenyl acts as a much more efficient transmitter than phenyl.

The UV–vis spectra of the Fe(III) complexes **3a** and **3c** display several absorptions which were found for all Fe(III) alkynyl complexes.[28] In particular, two distinct peaks are apparent in the 800–1050 nm range at the border between the visible and near-infrared range. For the related Fe(III) complexes of the 4-phenylethynyl series, corresponding absorptions were observed in the 600–850 nm spectral range and attributed to LMCT transitions.[28]

Measurements in the NIR range confirm the transparency of the Fe(II) complexes while the spectra of Fe(III) counterparts **3a**[PF_6] and **3c**[PF_6] present a weak absorption in the 1500–2000 nm range. As evidenced for **1a**[PF_6] and **1c**[PF_6] this absorption characteristic of Fe(III) complexes is reminiscent of a forbidden metal-centered ligand field electronic transition.[28]

7. Luminescence Spectroscopy. Upon excitation at $\lambda \geq 350$ nm at room temperature, the CH_2Cl_2 solutions of the anthracenyl complexes **2**, **2**[PF_6], **2**[PF_6]$_2$, **3a**, **3a**[PF_6], **3c**, and **3c**[PF_6] emit in the blue region. The emission spectra of these complexes are dominated by high-energy emission bands at ca. 404−472 nm and some of them with vibronic structures. For the mononuclear complexes **3a**, **3a**[PF_6], **3c**, and **3c**[PF_6], in general, the cyano-substituted complexes (i.e., **3c** and **3c**[PF_6]) emit at lower energies relative to their corresponding unsubstituted counterparts (i.e., **3a** and **3a**[PF_6]). In addition, the Fe(III) complexes (i.e., **3a**[PF_6] and **3c**[PF_6]) show slight red shifts in emission energies relative to the Fe(II) counterparts (i.e., **3a** and **3c**) as shown in Figure 2. These observations are probably the results of the electron-withdrawing properties of the cyano and the Fe(III) groups on the anthracenyl moieties. Similar findings were also observed in the low-temperature glass state emission spectra. The dinuclear complexes **2**, **2**[PF_6], and **2**[PF_6]$_2$ were found to emit at nearly identical wavelengths and band shapes both in room temperature solution state and low-temperature glass state, indicating that the [Fe(dppe)Cp*] moieties have little influence on the emission energies of this class of anthracenyl alkynyl complexes. Since emission bands with similar vibronic structures and energies were observed in the corresponding free ligands, the highly structured emission bands of these anthracenyl alkynyl complexes with lifetime <0.1 μs at room temperature were tentatively assigned as the ligand-centered emission of the alkynyl anthracene units. The luminescence quantum yields of these anthracenyl complexes are much lower than that of anthracene ($\Phi_{em} \approx 0.3$) and are nearly independent of the oxidation states of the iron moieties. Such a reduction in luminescence quantum yield in the anthracenyl complexes could be rationalized by the introduction of low-lying nonemissive excited states upon incorporation of the transition metal moieties which quenched the emission. Reduc-

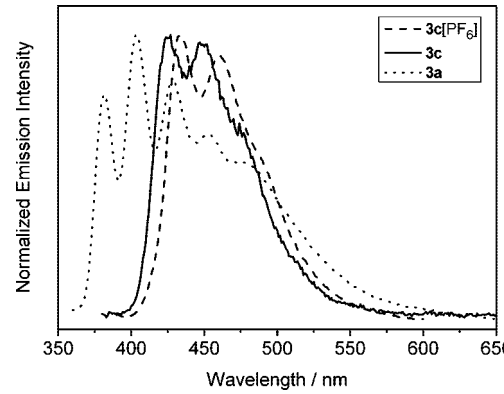

Figure 2. Normalized emission spectra of **3a**, **3c**, and **3c**[PF_6] in degassed dichloromethane at room temperature.

tive electron transfer quenching is also favorable in these Fe(II) complexes. From the electrochemical data, the Fe(II) moieties of complexes **3a** and **3c** can be readily oxidized to Fe(III) at −0.13 and +0.02 V vs SCE, respectively. With the structurally related compound dicyanoanthracene having an excited state reduction potential $E°(An*/An^{-\bullet})$ of about +2.00 V vs SCE,[68] positive values of $\Delta E°$ for the reductive quenching process by the Fe(II) moieties were obtained, indicating that, from a thermodynamic point of view, intramolecular reductive electron transfer quenching is a possible quenching mechanism for these anthracenyl iron(II) complexes. On the other hand, the presence of low-lying LMCT states in the Fe(III) alkynyl moieties, as reflected by the presence of the low-energy NIR absorptions, is capable of quenching the anthracene unit via an energy transfer pathway. Thus the luminescence quantum yields of both the Fe(II) and Fe(III) complexes are low and are rather insensitive toward the oxidation state of the Fe center, which is in contrast to our previous work on the mixed-metal complexes of iron and rhenium,[8] in which the luminescence quantum yield of the low-energy MLCT emission of the complex is dependent on the oxidation state of the iron moiety. The relatively high-energy anthracene ^{1}IL emissions observed in these anthracenyl iron alkynyl complexes could probably be quenched by both Fe(II) and Fe(III) moieties and that accounts for the relatively low luminescence quantum yield of all the complexes in this study.

Conclusion

We have reported here the synthesis, isolation, and characterization of several neutral and radical cation complexes of the formula $[(\eta^2\text{-dppe})(\eta^5\text{-}C_5Me_5)Fe(-C{\equiv}C\text{-}9,10\text{-ant-}X)]^{n+}n[Y]$ (ant = anthracene; n = 0, 1; **3a**^{n}Y, X = H; **3b**^{n}Y, X = Br; **3c**^{n}Y, X = CN; **3d**, X = C≡C−Si^{i}Pr$_3$; **3e**, X = C≡C−H; Y = PF_6^-, $TCNE^-$, $TCNQ^-$). An extensive analysis of the properties of this new family of molecules including redox potentials, X-ray determination, and Mössbauer, ESR, vibrational, and electronic spectroscopies was achieved. Comparison of these data with those previously obtained for the mononuclear complexes $[(\eta^2\text{-dppe})(\eta^5\text{-}C_5Me_5)Fe(C{\equiv}C{-}C_6H_4X)]^{n+}n[Y]$[26] clearly indicates that the anthracene enhances the cumulenic character of the bonding and increases the sensitivity to the electronic properties of the remote substituent X. As a result, the 9,10-anthracenyl bridge acts as a much more efficient transmitter than phenyl. Mössbauer and ESR data do not suggest a significant spin distribution onto the ethynylanthracenyl ligand, but a strong metal character for these radicals.

Despite the bulkiness of the iron building block that pushes the anthracene rings further apart, it was shown that these forces can be counter balanced by cation–anion interactions. Indeed, analysis of the crystal structure of **3c**[TCNE] reveals an intermolecular $\pi-\pi$ stacking between the anthracenes rings.

These Fe(II) and Fe(III) complexes exhibit weaker luminescence property than the free carbon-rich ligand. It was shown that both Fe(II) and Fe(III) moieties can quench the ligand-centered emission by two different pathways.

Experimental Section

General Data. All the manipulations were carried out under an argon atmosphere with Schlenk techniques or in a Jacomex 532 drybox filled with argon. Routine NMR spectra were recorded with a Bruker DPX 200 spectrometer. High-field NMR spectral experiments were performed on a multinuclear Bruker WB 300 instrument. Chemical shifts are given in parts per million relative to tetramethylsilane (TMS) for ^{1}H and ^{13}C NMR spectra, and H_3PO_4 for ^{31}P NMR spectra. X-Band ESR spectra were recorded on a Bruker ESP-300E spectrometer. An Air Products LTD-3-110 liquid helium transfer system was attached for the low-temperature measurements. Transmittance FTIR spectra were recorded with a Bruker IFS128 spectrometer (400–7500 cm^{-1}). Liquid near-infrared spectra were recorded on a Cary 5 spectrometer. UV–visible spectra were recorded on an UVIKON XL spectrometer. The ^{57}Fe Mössbauer spectra were obtained by using a constant acceleration spectrometer previously described with a 50 mCi ^{57}Co source in a Rh matrix. The sample temperature was controlled by a Oxford MD306 cryostat and an Oxford ITC4 temperature controller. Computer fitting of the Mössbauer data to Lorenzian line shapes were carried out with a previously reported computer program. The isomer shift values are reported with respect to iron foil at 298 K and are not corrected for the temperature-dependent second-order Doppler shift. The Mössbauer sample cell consists of a 2 cm diameter cylindrical plexiglass holder. Steady state excitation and emission spectra were obtained on a Spex Fluorolog 111 spectrofluorometer. Elemental analyses were performed at the CRMPO, University of Rennes 1, France.

$(\eta^2$-dppe$)(\eta^5$-C$_5$Me$_5$)FeC≡C-ant-H (3a). A mixture of $(\eta^2\text{-dppe})(\eta^5\text{-}C_5Me_5)Fe{-}C{\equiv}C{-}H$ **8** (0.27 g, 0.44 mmol), 9-iodoanthracene **9** (134 mg, 0.44 mmol), $PdCl_2(PPh_3)_2$ (31 mg, 0.044 mmol), and CuI (17 mg, 0.089 mmol) in THF (20 mL) and HN^{i}Pr$_2$ (20 mL) was stirred at 70 °C for 12 h to give a raspberry solution. After evaporation to dryness, the crude product was dissolved in toluene and passed through a short pad of neutral alumina oxide under argon. Removal of the solvents gave a solid that was washed twice with pentane to afford pure complex **3a** as a raspberry powder. Yield: 0.25 g (71%). Anal. Calcd for $C_{52}H_{48}FeP_2$: C, 78.98; H, 6.12. Found: C, 78.12; H, 6.07. FT-IR (Nujol, cm^{-1}): 2022 ($\nu_{C\equiv C}$). UV–vis (CH_2Cl_2): λ_{max} (ϵ) 553 (5708), 391 (5682), 371 (5944), 260 (55863). ^{1}H NMR (200 MHz, C_6D_6): δ 8.35 (d, 2 H, Ant, J = 8 Hz), 7.96–7.84 (m, 7 H, Ant and Ph), 7.33–6.98 (m, 20 H, Ant and Ph), 2.95 (m, 2 H, CH_2), 1.92 (m, 2 H, CH_2), 1.63 (s, 15 H, Cp*). ^{31}P NMR (81 MHz, C_6D_6): δ 101.8 (s, dppe). CV (CH_2Cl_2, 20 °C, 0.1 M ^{n}Bu$_4$NPF$_6$, υ = 0.1 V/s): $E°$ = −0.135 V (ΔE_p = 0.069 V, i_c/i_a = 1.0). High-resolution MS (FAB) m/z 790.2580 (calcd for $C_{52}H_{48}{}^{56}FeP_2$ 790.2581).

$(\eta^2$-dppe$)(\eta^5$-C$_5$Me$_5$)FeC≡C-ant-Br (3b). $[(\eta^2\text{-dppe})(\eta^5\text{-}C_5Me_5)FeC{\equiv}C\text{-ant-Br}][PF_6]$ (**3b**[PF$_6$], 740 mg, 0.73 mmol) and ^{t}BuOK (90 mg, 0.80 mmol) in THF (50 mL) were stirred for 5 h at room temperature. After evaporation to dryness, the crude product was dissolved in ether and passed through a short pad of celite under argon. The solid was dried under vacuum to give pure complex **3b** as a dark red powder. Yield: 0.560 g (87%). FT-IR (Nujol, cm^{-1}): 2011 ($\nu_{C\equiv C}$). CV (CH_2Cl_2, 20 °C, 0.1 M ^{n}Bu$_4$NPF$_6$, υ = 0.1 V/s): $E°$ = −0.083 V (ΔE_p = 0.090 V, i_c/i_a = 1.0). UV–vis (CH_2Cl_2): λ_{max} (ϵ) 592 (6621), 392 (4830), 266 (53250). ^{1}H NMR (200 MHz, C_6D_6): δ 8.79 (d, 2 H, Ant, J = 9 Hz), 8.44 (d, 2 H, Ant, J = 9 Hz), 8.03–7.93 (m, 5 H, Ph), 7.45–7.01 (m, 19 H, Ant and Ph), 2.96 (m, 2 H, CH_2), 2.02 (m, 2 H, CH_2), 1.69 (s, 15 H, Cp*). ^{31}P NMR (81 MHz, C_6D_6): δ 101.2 (s, dppe). High-resolution MS (FAB) m/z 868.1716 (calcd for $C_{52}H_{47}{}^{56}FeBrP_2$ 868.1686). X-ray-quality crystals of $(\eta^2$-dppe$)(\eta^5$-C^{5}Me^5)FeC≡C-9,10-ant-Br were grown by slow evaporation of a pentane solution of the above compound.

$(\eta^2$-dppe$)(\eta$5-C5Me5)FeC≡C-ant-C≡N (3c). A mixture of $(\eta^2\text{-dppe})(\eta^5\text{-}C_5Me_5)FeC{\equiv}CH$ **8** (0.50 g, 0.81 mmol), 9-bromo-10-cyanoanthracene **5c** (0.23 g, 0.81 mmol), $PdCl_2(PPh_3)_2$ (57 mg, 0.081 mmol), and CuI (31 mg, 0.163 mmol) in THF (30 mL) and HN^{i}Pr$_2$ (20 mL) was stirred at room temperature for 12 h to give a deep blue solution. After evaporation to dryness, the crude product was dissolved in toluene and passed through a short pad of neutral

(68) Ci, X.; Whitten, D. G. *J. Phys. Chem.* **1991**, *95*, 1988–1993.

alumina oxide under argon. Removal of the solvents gave a solid that was washed twice with pentane to afford pure complex **3c** as a blue powder. Yield: 0.55 g (83%). Anal. Calcd for $C_{53}H_{47}FeNP_2 \cdot CH_2Cl_2$: C, 72.01; H, 5.48. Found: C, 71.00; H, 5.38. FT-IR (Nujol, cm^{-1}): 2194 ($\nu_{C\equiv N}$), 1986 ($\nu_{C\equiv C}$). UV–vis (CH_2Cl_2): λ_{max} (ϵ) 651 (16684), 411 (6351), 391 (6439), 320 (13951), 268 (71216). ^{1}H NMR (200 MHz, C_6D_6): δ 8.55 (d, 2 H, Ant, $J = 8$ Hz), 8.21 (d, 2 H, Ant, $J = 8$ Hz), 7.80 (m, 4 H, Ph), 7.29–6.87 (m, 20 H, Ant and Ph), 2.78 (m, 2 H, CH_2), 1.92 (m, 2 H, CH_2), 1.55 (s, 15 H, Cp*). ^{31}P NMR (81 MHz, C_6D_6): δ 100.8 (s, dppe). CV (CH_2Cl_2, 20 °C, 0.1 M ^{n}Bu$_4$NPF$_6$, $\upsilon = 0.1$ V/s): $E^\circ = 0.016$ V ($\Delta E_p = 0.086$ V, $i_c/i_a = 1.0$). High-resolution MS (FAB) *m/z* 815.2534 (calcd for $C_{53}H_{47}{}^{56}FeNP_2$ 815.2533). X-ray-quality crystals of (η^2-dppe)(η^5-C_5Me_5)FeC≡C-9,10-Ant-C≡N $\cdot$ CH_2Cl_2 were grown by slow diffusion of pentane into a saturated CH_2Cl_2 solution of the above compound.

(η^2-dppe)(η^5-C_5Me_5)FeC≡C-ant-C≡CSi^{i}Pr$_3$ (3d). In a Schlenk tube wrapped with aluminum foil, 9-triisopropylsilylethynyl-10-ethynylanthracene obtained from **4d** (300 mg, 0.77 mmol) in 50 mL of methanol and 20 mL of THF were stirred in the presence of 1.1 equiv of (η^2-dppe)(η^5-C_5Me_5)FeCl (**6**, 0.57 g, 0.92 mmol) and 1.1 equiv of $NaBPh_4$ (315 mg, 0.92 mmol). After approximately 16 h of stirring, ^{t}BuOK (96 mg, 1.1 equiv) was introduced. Stirring was maintained for 4 h before the solvent was removed. The residue was extracted with toluene (3 × 30 mL) and passed through a short pad of neutral aluminum oxide under argon to afford pure complex **3d** as a dark red powder. Yield: 0.43 g (57%). FT-IR (Nujol, cm^{-1}): 2118 and 1998 (s and w, $\nu_{C\equiv C}$). CV (CH_2Cl_2, 20 °C, 0.1 M ^{n}Bu$_4$NPF$_6$, $\upsilon = 0.1$ V/s): $E^0 = -0.097$ V ($\Delta E_p = 0.080$ V; $i_c/i_a = 1.0$). UV–vis (CH_2Cl_2): λ_{max} (ϵ) 613 (2610), 423 (2850), 400 (3040), 256 (37330). ^{1}H NMR (200 MHz, C_6D_6): δ 9.02 (d, 2 H, Ant, $J = 8$ Hz), 8.32 (d, 2 H, Ant, $J = 8$ Hz), 7.45–7.30 (m, 4 H, Ph), 7.25–6.90 (m, 20 H, Ant and Ph), 2,88 (m, 2 H, CH_2), 1.96 (m, 2 H, CH_2), 1,61 (s, 15 H, C$_5$(CH_3)$_5$), 1,34 (s, 21 H, Si^{i}Pr$_3$). ^{31}P NMR (81 MHz, C_6D_6): δ 101,4 (s, dppe). High-resolution MS (FAB) *m/z* 970.3915 (calcd for $[C_{63}H_{68}SiP_2{}^{56}Fe]^+$ 970.3918).

(η^2-dppe)(η^5-C_5Me_5)FeC≡C-ant-C≡CH (3e). In a Schlenk tube wrapped with aluminum foil, (η^2-dppe)(η^5-C_5Me_5)Fe—C≡C-ant-C≡C—Si^{i}Pr$_3$ **3d** (300 mg, 0.31 mmol) in 60 mL of THF was stirred in the presence of 0.3 equiv of TBAF (0.09 mL g, 0.09 mmol) for 16 h at 50 °C before the solvent was removed. The residue was extracted with ether (4 × 50 mL) and passed through a short pad of silica under argon to afford complex **3e** as a dark red powder. Yield: 208 mg (82%). FT-IR (Nujol, cm^{-1}): 3304 (m, $\nu_{\equiv C-H}$), 2111 and 2011 (s and w, $\bar{\nu}_{C\equiv C}$). CV (CH_2Cl_2, 20 °C, 0.1 M ^{n}Bu$_4$NPF$_6$, $\upsilon = 0.1$ V/s): $E^0 = -0.112$ V ($\Delta E_p = 0.050$ V; $i_c/i_a = 1.0$). ^{1}H NMR (200 MHz, C_6D_6): δ 8.75 (d, 2 H, Ant, $J = 8$ Hz), 8.15 (d, 2 H, Ant, $J = 8$ Hz), 8.00–7.75 (m, 4 H, Ph), 7.25–6.90 (m, 20 H, Ant and Ph), 3.73 (s, 1 H, C≡C—*H*), 3.00 (m, 2 H, CH_2), 2,05 (m, 2 H, CH_2), 1.68 (s, 15 H, C$_5$(CH_3)$_5$). ^{31}P NMR (81 MHz, C_6D_6): δ 101,8 (s, dppe).

[(η^2-dppe)(η^5-C_5Me_5)FeC≡C-ant-H][PF$_6$] (3a[PF$_6$]). Complex (η^2-dppe)(η^5-C_5Me_5)FeC≡C-9-ant-H **3a** (200 mg , 0.253 mmol) and [$FeCp_2$][PF_6] (79 mg, 0.240 mmol) in THF (30 mL) were stirred for 2 h at −80 °C. After evaporation of the solvents, the residue was dissolved in CH_2Cl_2 and precipitated by addition of Et_2O. After a second partial precipitation with CH_2Cl_2 and Et_2O, the solid was dried under vacuum to give pure complex **3a**[PF_6] as a dark blue powder. Yield: 0.191 g (85%). FT-IR (Nujol, cm^{-1}): 2018 ($\nu_{C\equiv C}$), 837 (ν_{P-F}). NIR (CH_2Cl_2, cm^{-1}): (ϵ, $\Delta\upsilon_{1/2}$) 11310 (700, 1000), 9880 (1030, 300), 5300 (100, 375). UV–vis (CH_2Cl_2): λ_{max} (ϵ) 604 (6000), 534 (5400), 418 (6800), 396 (8200), 373 (7600), 266 (52800), 259 (52500), 231 (48100). CV (CH_2Cl_2, 20 °C, 0.1 M ^{n}Bu$_4$NPF$_6$, $\upsilon = 0.1$ V/s): $E^\circ = -0.134$ V ($\Delta E_p = 0.080$ V, $i_c/i_a = 1.0$). ESR (CH_2Cl_2/$C_2H_4Cl_2$ 1/1, 77 K): $g_x = 2.412$; $g_y = 2.037$; $g_z = 1.978$. High-resolution MS (FAB) *m/z* 790.2559 (calcd for $[C_{52}H_{48}{}^{56}FeP_2]^+$ 790.2581).

[(η^2-dppe)(η^5-C_5Me_5)FeC≡C-ant-Br][PF$_6$] (3b[PF$_6$]). Method A: A mixture of (η^2-dppe)(η^5-C_5Me_5)FeC≡CH **8** (980 mg, 1.61 mmol), 9,10-dibromoanthracene **5b** (590 mg, 1.76 mmol), $PdCl_2(PPh_3)_2$ (112 mg, 0.16 mmol), CuI (61 mg, 0.32 mmol), and HN^{i}Pr$_2$ (50 mL) was stirred at 50 °C for 2 days. After evaporation to dryness, the crude product was dissolved in ether and passed through a short pad of celite under argon. After evaporation to dryness, [$FeCp_2$][PF_6] (260 mg, 0.80 mmol) in THF (30 mL) was added. Then the mixture was stirred for 3 h at –80 °C. After evaporation of the solvents, the residue was dissolved in CH_2Cl_2 and precipitated by addition of Et_2O. After a second partial precipitation with CH_2Cl_2 and Et_2O, the solid was dried under vacuum to give pure complex **3b**[PF_6] as a black powder. Yield: 0.742 g (45%). **Method B:** In a Schlenk tube wrapped with aluminum foil, 10-bromo-9-trimethylsilylethynylanthracene **4b** (350 mg, 0.99 mmol) in 50 mL of methanol were stirred for 6 h in the presence of 1.1 equiv of potassium carbonate (150 mg, 1.09 mmol). Then 1.1 equiv of (η^2-dppe)(η^5-C_5Me_5)FeCl **6** (681 mg, 1.09 mmol) and 1.1 equiv of $NaBPh_4$ (373 mg, 1.09 mmol) were added. After approximately 16 h of stirring, ^{t}BuOK (122 mg, 1,1 equiv) was introduced. Stirring was maintained for 4 h before the solvent was removed. After evaporation to dryness, the crude product was dissolved in ether and passed through a short pad of celite under argon. After evaporation to dryness, [$FeCp_2$][PF_6] (230 mg, 0.70 mmol) in THF (30 mL) was added. Then the mixture was stirred for 3 h at –80 °C. After evaporation of the solvents, the residue was dissolved in CH_2Cl_2 and precipitated by addition of Et_2O. After a second partial precipitation with CH_2Cl_2 and Et_2O, the solid was dried under vacuum to give pure complex **3b**[PF_6] as a black powder. Yield: 0.370 g (43%). FT-IR (Nujol, cm^{-1}): 1957 ($\nu_{C\equiv C}$),; 837 (ν_{P-F}). CV (CH_2Cl_2, 20 °C, 0.1 M ^{n}Bu$_4$NPF$_6$, $\upsilon = 0.1$ V/s): $E^\circ = -0.083$ V ($\Delta E_p = 0.090$ V, $i_c/i_a = 1.0$). UV–vis (CH_2Cl_2): λ_{max} (ϵ) 579 (2511), 432 (9111), 408 (8513), 271 (63080). Mössbauer (mm/s vs Fe, 80 K): IS 0.116, QS 0.927. High-resolution MS (FAB) *m/z* 868.1704 (calcd for $C_{52}H_{47}{}^{56}FeBrP_2$ 868.1686).

[(η^2-dppe)(η^5-C_5Me_5)FeC≡C-ant-C≡N][PF$_6$] (3c[PF$_6$]). Complex (η^2-dppe)(η^5-C_5Me_5)FeC≡C-9,10-ant-C≡N **3c** (200 mg, 0.245 mmol) and [$FeCp_2$][PF_6] (77 mg, 0.233 mmol) in THF (30 mL) were stirred for 3 h at −80 °C. After evaporation of the solvents, the residue was dissolved in CH_2Cl_2 and precipitated by addition of Et_2O. After a second partial precipitation with CH_2Cl_2 and Et_2O, the solid was dried under vacuum to give pure complex **3c**[PF_6] as a brown powder. Yield: 0.194 g (87%). FT-IR (Nujol, cm^{-1}): 2207 ($\nu_{C\equiv N}$), 1976 ($\nu_{C\equiv C}$), 833 (ν_{P-F}). NIR (CH_2Cl_2, cm^{-1}): (ϵ, $\Delta\upsilon_{1/2}$) 11160 (1040, 1000), 9765 (1360, 325), 5065 (270, 350). UV–vis (CH_2Cl_2): λ_{max} (ϵ) 537 (9100), 441 (16400), 272 (59600), 232 (34900). CV (CH_2Cl_2, 20 °C, 0.1 M *n*-Bu_4NPF_6, $\upsilon = 0.1$ V/s): $E^\circ = 0.027$ V ($\Delta E_p = 0.078$ V, $i_c/i_a = 1.0$). X-ray-quality crystals of [(η^2-dppe)(η^5-C_5Me_5)FeC≡C-9,10-ant-C≡N][PF_6] were grown by slow diffusion of pentane into a saturated CH_2Cl_2 solution of the above compound.

[(η^2-dppe)(η^5-C_5Me_5)FeC≡C-ant-C≡N][TCNE] (3c[TCNE]). Complex (η^2-dppe)(η^5-C_5Me_5)FeC≡C-9,10-ant-C≡N **3c** (150 mg, 0.184 mmol) and 23.5 mg of TCNE (0.184 mmol) in THF (20 mL) were stirred for 2 h at –80 °C. After evaporation of the solvents, the residue was dissolved in CH_2Cl_2 and precipitated by addition of Et_2O. After filtration, the solid material was washed with Et_2O and dried under vacuum to give pure complex **3c**[TCNE] as a brown powder. Yield: 0.14 g (81%). Anal. Calcd for $C_{59}H_{47}FeN_5P_2$: C, 75.08; H, 5.02. Found: C, 74.80; H, 4.98. FT-IR (Nujol, cm^{-1}): 2217 ($\nu_{C\equiv N}$), 2183 ($\nu_{C\equiv N}$), 2144 ($\nu_{C\equiv N}$), 1977 ($\nu_{C\equiv C}$). NIR (CH_2Cl_2, cm^{-1}): (ϵ, $\Delta\upsilon_{1/2}$) 11210 (920, 1000), 9765 (1270, 325), 5060 (250, 400). UV–vis (CH_2Cl_2): λ_{max} (ϵ) 538 (8600), 439 (21400), 273 (61900), 234 (42800). CV (CH_2Cl_2, 20 °C, 0.1 M ^{n}Bu$_4$NPF$_6$, $\upsilon = 0.1$ V/s): $E^\circ_1 = 0.263$ V ($\Delta E_p = 0.074$ V, $i_c/i_a = 1.0$); $E^\circ_2 = 0.017$ V ($\Delta E_p = 0.070$ V, $I_p{}^a/I_p{}^c = 1.0$); $E^\circ_3 = -0.758$ V ($\Delta E_p = 0.108$ V, $I_p{}^a/I_p{}^c = 1.0$). X-ray-quality crystals of [(η^2-dppe)(η^5-C_5Me_5)FeC≡C-

9,10-ant-C≡N][TCNE] were grown by slow diffusion of pentane into a saturated CH_2Cl_2 solution of the above compound.

[(η^2-dppe)(η^5-C_5Me_5)FeC≡C-ant-C≡N][TCNQ] (3c[TCNQ]). Complex (η^5-C_5Me_5)(dppe)FeC≡C-9,10-ant-C≡N **3c** (200 mg, 0.245 mmol) and 50 mg of TCNQ (0.245 mmol) in THF (20 mL) were stirred for 2 h at –80 °C. After evaporation of the solvents, the residue was dissolved in CH_2Cl_2 and the temperature was decreased to –80 °C to allow the precipitation of the product by addition of Et_2O. After a second partial precipitation with CH_2Cl_2 and Et_2O at low temperature, the solid was dried under vacuum to give pure complex **3c**[TCNQ] as a black powder. Yield: 0.205 g (82%). FT-IR (Nujol, cm^{-1}): 2212 ($\nu_{C\equiv N}$), 2178 ($\nu_{C\equiv N}$), 2151 ($\nu_{C\equiv N}$), 1951 ($\nu_{C\equiv C}$). NIR (CH_2Cl_2, cm^{-1}): (ϵ, $\Delta\upsilon_{1/2}$) 9765 (1135, 325), 5065 (215, 400). UV–vis (CH_2Cl_2): λ_{max} (ϵ) 851 (29300), 831 (20000), 768 (14200), 750 (17400), 733 (12500), 542 (8400), 435 (24200), 421 (29700), 404 (40100), 273 (65600), 235 (38400). CV (CH_2Cl_2, 20 °C, 0.1 M ^{n}Bu_4NPF_6, υ = 0.1 V/s): E°_1 = 0.207 V (ΔE_p = 0.085 V, I_p^a/I_p^c = 1.0); E°_2 = 0.020 V (ΔE_p = 0.090 V, I_p^a/I_p^c = 1.0); E°_3 = –0.368 V (ΔE_p = 0.075 V, i_c/i_a = 1.0). X-ray-quality crystals of [(η^2-dppe)(η^5-C_5Me_5)FeC≡C-9,10-ant-C≡N]-[TCNQ] were grown by slow diffusion of pentane into a saturated THF solution of the above compound.

Acknowledgment. We acknowledge the award of a grant by CNRS/RGC under the PROCORE: France-Hong Kong Joint Research Scheme (Project No. 09281 QE). F.d.M. acknowledges the Ministry of Research and Education for a fellowship.

Supporting Information Available: CIF files for **3b**, **3c**, **3c[PF_6]**, **3c[TCNE]**, and **3c[TCNQ]**. This material is available free of charge via the Internet at http://pubs.acs.org.

OM701278E